Discover Oncology

Research

Timosaponin B-II suppresses gastric cancer cell proliferation and induces apoptosis via the Nrf2/miR-455-3p/KLF6 pathway

Qiaoyan Cui[1] · Ruijie Zhang[2] · Shiqiao Zhao[3] · Jian Wang[1] · Yafen Dong[1] · Xuesong Bai[1] · Ye Chen[1] · Yan Qiu[1]

Received: 6 February 2025 / Accepted: 9 May 2025
Published online: 23 May 2025

Abstract

Background Gastric cancer (GC), known for its aggressive growth and metastasis, remains a leading cause of cancer-related mortality. Although Timosaponin B-II (TB-II) from *Anemarrhena asphodeloides* has shown anticancer potential, its underlying mechanisms in GC are not yet fully understood.

Methods Our study investigates and compares the expression patterns of Kruppel-Like Factor 6(KLF6) in GC tissues across different TNM stages, while exploring its upstream regulatory factors. GC cells were treated with Timosaponin B-II (TB-II), and alterations in cell proliferation and apoptosis rates were evaluated using CCK-8 and TUNEL assays. Furthermore, the expression levels of nuclear factor erythroid 2-related factor 2(Nrf2), miR-455-3p, and KLF6 were quantified to elucidate the mechanisms underlying TB-II's effects. To confirm the interaction between miR-455-3p and KLF6, as well as Nrf2 and miR-455-3p, bioinformatics analysis, luciferase assays, and ChIP-PCR were conducted. Finally, protein synthesis and degradation assays were performed to explore the mechanism by which TB-II regulates the expression and activity of Nrf2.

Results Both mRNA and protein expression levels of KLF6 were significantly lower in GC tissues compared to adjacent normal tissues. Notably, only KLF6 protein expression exhibited a decline in GC tissues from stages I to III of GC, whereas its upstream regulator, miR-455-3p, displayed the opposite trend. Treatment with TB-II markedly inhibited GC cells proliferation and induced apoptosis in a dose-dependent manner. Mechanistically, TB-II treatment upregulated the expression of Kelch-like ECH-associated protein 1(Keap1) protein, facilitating the formation of the Keap1/Nrf2 complex, which enhanced the ubiquitin-mediated degradation of Nrf2 in GC cells. Consequently, the transcriptional activation of miR-455-3p by Nrf2 was suppressed, resulting in the upregulation of the tumor suppressor KLF6. Silencing KLF6 can counteract the effects of TB-II in inhibiting proliferation and promoting apoptosis in GC cells.

Conclusion TB-II suppresses GC cell proliferation and induces apoptosis via the Nrf2/miR-455-3p/KLF6 pathway.

Keywords Timosaponin B-II · Gastric cancer(GC) · Nrf2 · miR-455-3p · KLF6

Qiaoyan Cui and Ruijie Zhang have contributed to the work equally.

Supplementary Information The online version contains supplementary material available at https://doi.org/10.1007/s12672-025-02650-9.

✉ Yan Qiu, qiuyan@shpdph.com | [1]Department of Pharmacy, Shanghai Pudong New Area People's Hospital, Shanghai 201299, China. [2]Tongji University School of Medicine, Shanghai, China. [3]Department of Environmental Health, Harvard University, Boston, MA, USA.

1 Introduction

Gastric cancer (GC) is among the most prevalent cancers worldwide, with a 5-year relative survival rate of approximately 20% [1]. In recent years, advancements in diagnostic techniques and clinical indicators have significantly improved the outcomes of GC patients. However, the overall survival rate for many patients remains poor, posing significant challenges [2]. As a result, the development of novel therapeutic strategies for GC remains urgent clinical priorities. Currently, chemotherapy is the mainstay of treatment for advanced GC. While molecularly targeted therapies and immunotherapeutic agents have shown initial promise, their application is often constrained by factors such as patient-specific drug responsiveness, emerging drug resistance, and adverse side effects. Therefore, the development of highly effective and low-toxicity anticancer drugs remains a central focus in GC prevention and treatment research [3].

Natural products and their derivatives have long been invaluable in the development of anti-tumor therapies, contributing to nearly 50% of all cancer drugs currently in use. These compounds, including alkaloids, polysaccharides, polyphenols, diterpenes, and unsaturated fatty acids, are highly regarded for their multi-targeted effects, potent bioactivity, and relatively low toxicity [4]. Natural compounds are recognized for their significant anticancer potential, attributed to their multi-targeted activities, potent bioactivity, and relatively low toxicity [5]. Among these, Timosaponin A-III, derived from *Anemarrhena asphodeloides*, has exhibited notable inhibitory effects against lung adenocarcinoma, breast cancer, and liver cancer [6, 7]. However, whether other bioactive components of Timosaponins possess similar efficacy against GC, particularly regarding their precise mechanisms of action, remains unclear and requires further systematic investigation. In this study, we will investigate the effects of TB-II on the proliferation and apoptosis of GC cells through in vitro experiments. We will also analyze the underlying mechanisms and, based on the changes in pathway components, preliminarily identify the target through which TB-II inhibits GC progression. Overall, we aim for this study to expand the potential applications of TB-II in cancer therapy, provide a theoretical foundation for its use in the prevention and treatment of GC, and identify target proteins that could serve as potential candidates for the design and development of more effective anticancer drugs based on TB-II as a prototype.

2 Materials and methods

2.1 Tumor tissue collection and analysis

Tumor tissues were collected from 36 GC patients with TNM stages I-III (12 patients per stage) at Shanghai Pudong New Area People's Hospital. Detailed clinicopathological information and tumor classification can be found in Table 1. There were no age restrictions for enrollment. The collection and use of tumor samples were conducted in compliance with ethical guidelines. All patients provided written informed consent. This study was approved by the Ethics Committee of Shanghai Pudong New Area People's Hospital (Approval Number: 2023-LW-09), in accordance with the Declaration of Helsinki and the International Ethical Guidelines for Biomedical Research Involving Human Subjects. During surgery, both tumor and adjacent normal tissue specimens were meticulously collected following strict protocols. Tumor samples were obtained from both the center and peripheral regions to ensure comprehensive representation, while adjacent normal tissues were collected from areas at least 2.5 cm away from the tumor. Both tissue types were immediately frozen in liquid nitrogen and stored at -80 °C for further analysis. Total RNA was extracted from both tumor and adjacent normal tissues to assess the expression levels of Nrf2, KLF6 mRNA, and miR-455-3p using Reverse Transcription-Quantitative Polymerase Chain Reaction (RT-qPCR). Total protein extracted from the same tissues was analyzed using Enzyme-Linked Immunosorbent Assay (ELISA) to measure Kruppel-Like Factor 6(KLF6) protein levels, employing the Human KLF6 ELISA kit (Cusabio, Beijing, China). Additionally, the correlation between KLF6 protein expression and miR-455-3p levels in GC tissues was evaluated.

2.2 Cell culture

The GC cell lines AGS and NCI-N87 were obtained from the American Type Culture Collection (ATCC, VA, USA). These cell lines, which exhibit adherent growth, were cultured in D-MEM (Thermofisher, MI, USA) supplemented with 10%

Table 1 Clinical and pathological characteristics of 36 gastric cancer patients

Gender	Age	TNM Stage-I	Tumor Location
Female	42	T1N0M0	Body
Male	66	T1N0M0	Antrum
Female	58	T1N0M0	Body
Female	64	T1N0M0	Cardia
Male	65	T1N0M0	Pylorus
Male	49	T2N0M0	Cardia
Male	59	T1N0M0	Antrum
Female	62	T1N1M0	Antrum
Female	66	T2N0M0	Antrum
Female	54	T1N0M0	Fundus
Male	52	T1N1M0	Cardia
Female	70	T1N0M0	Body
Gender	Age	TNM Stage-II	Tumor Location
Male	55	T3N1M0	Fundus
Female	64	T1N2M0	Cardia
Female	43	T2N2M0	Fundus
Female	68	T1N2M0	Antrum
Male	62	T3N1M0	Cardia
Male	65	T3N1M0	Body
Female	54	T2N1M0	Antrum
Female	68	T3N2M0	Cardia
Male	72	T2N2M0	Body
Female	52	T3N1M0	Antrum
Male	46	T2N1M0	Pylorus
Female	53	T2N2M0	Cardia
Gender	Age	TNM Stage-III	Tumor Location
Female	52	T3N2M0	Antrum
Male	63	T3N2Mx	Pylorus
Male	45	T3N3M0	Antrum
Female	61	T4N3M0	Cardia
Female	54	T3N2M0	Antrum
Male	43	T3N3M0	Body
Male	52	T4N3M0	Body
Female	73	T3N2Mx	Antrum
Male	58	T3N2M0	Fundus
Female	62	T4N2M0	Body
Female	52	T4N3M0	Body
Male	67	T4N3M0	Body

The TNM staging for gastric cancer is primarily based on the guidelines set by the American Joint Committee on Cancer (AJCC) (9th Edition) and the Union for International Cancer Control (UICC) (8th Edition), both published in 2017. These staging systems assess the severity of gastric cancer based on tumor size (T), lymph node involvement (N), and the presence of distant metastasis (M). All enrolled patients had tumors classified as adenocarcinoma

fetal bovine serum (FBS, Thermofisher) and maintained at 37 °C in a humidified incubator (MCO-20AIC, SANYO, Japan) with 95% air and 5% CO_2. Upon reaching approximately 75% confluency, the cells were detached using 0.25% trypsin (Thermofisher) and subcultured to maintain optimal growth conditions.

2.3 Proliferation and TUNEL staining analysis

The experiment was simultaneously conducted in both AGS and NCI-N87 cell lines. The experimental groups were as follows: (1) Control group (no treatment); (2) Solvent group (cells were treated with DMSO at the same volume as used in the TB-II groups); (3) LD(Low-dose)-TB-II group (cells were treated with TB-II at a final concentration of 1 μg/ml); (4) HD(High-dose)-TB-II group (cells were treated with TB-II at a final concentration of 5 μg/ml); (5) Lv-NC+HD-TB-II group (cells were infected with Lv-NC and treated with TB-II at a final concentration of 5 μg/ml); and(6) Lv-shRNA-KLF6+HD-TB-II group (cells were infected with Lv-shRNA-KLF6 and treated with TB-II at a final concentration of 5 μg/ml). Recombinant lentivirus Lv-shRNA-KLF6 (Wzbio, Shandong, China) was used to specifically silence KLF6 in GC cells. Following infection with Lv-shRNA-KLF6 and Lv-NC, siRNA-KLF6 (5′-GUUUACCUCCGACCCCAUU-3′) and its scrambled sequence (NC, 5′-CGUCUCCAUUACUCAGUCC-3′) were generated in GC cells. Lentiviral infection was completed 72 h prior to TB-II (XG-7726, Sig Biotechnology Co., Ltd, Shanghai, China) treatment. After 48 h of TB-II treatment, the cells were used for proliferation and TUNEL assays. For the proliferation assay, cells were seeded into 96-well culture plates at a density of 1×10^4 cells per well, they were cultured in completely medium under normal conditions. Cell proliferation activity was assessed using the CCK-8 assay at 24,48 and 72 h post-culture. To evaluate cell proliferation, 10 μL of CCK-8 reagent (Abcam, Cambridge, UK) was added to each well, and the 96-well plate was gently shaken to ensure thorough mixing. The plate was then incubated at 37 °C for 2 h. Following incubation, the absorbance (OD value) of each well was measured at 450 nm using a microplate reader (ELx808IU, BioTek, VT, USA). The OD value is directly proportional to cell proliferation activity. For apoptosis analysis, these GC cells from each treatment group were re-seeded into 6-well plates at a density of 1×10^5 cells per well. The cells were cultured overnight in complete medium under standard conditions to allow for full adhesion. Afterward, the cells were fixed with 4% paraformaldehyde (PFA) for 20 min. Following fixation, the cells were permeabilized with 0.1% Triton X-100 in dPBS for 8 min. Next, according to the TUNEL staining kit (C1090, Beyotime, Shanghai, China) instructions, the TUNEL reaction mixture was added, and the cells were incubated at 37 °C for 1 h. During this incubation, the TdT enzyme incorporated the labeled dUTP into the 3′ ends of DNA breaks, thereby marking apoptotic cells. Once the staining reaction was complete, the cells were washed with dPBS to remove any unbound reagents, followed by 4′,6-diamidino-2-phenylindole (DAPI) staining to label the cell nuclei. Finally, the stained cells were observed using fluorescence microscopy. Apoptotic cells, marked by TUNEL, appeared as red fluorescence.

2.4 Impact of TB-II treatment on Nrf2, KLF6, and miR-455-3p expression in GC cells

AGS and NCI-N87 cells in the logarithmic growth phase were digested with 0.25% trypsin, resuspended in complete medium, and adjusted to a concentration of 5×10^4 cells/ml. The cells were seeded into 6-well culture plates at a volume of 2 ml per well. After overnight incubation under standard conditions, the cells were randomly divided into four groups: (1) Control group (no treatment); (2) Solvent group (treated with DMSO at the same volume as used in TB-II groups); (3) LD-TB-II group (Treated with TB-II at a final concentration of 1 μg/ml); (4) HD-TB-II group (Treated with TB-II at a final concentration of 5 μg/ml). After 48 h of TB-II treatment, the expression levels of miR-455-3p, Nrf2, and KLF6 were analyzed using RT-qPCR and western blotting.

2.5 Luciferase assay

The binding sites of miR-455-3p in the 3′ Untranslated Region (3′-UTR) of human KLF6 mRNA were predicted using "TargetScan 7.1" (Bartel Laboratory, Massachusetts Institute of Technology, MI, USA). The 3′-UTR of KLF6 was amplified and cloned to construct pGL3-wt-KLF6, which contains a luciferase reporter system composed of firefly luciferase and the KLF6 3′-UTR. The 293 cells were seeded at a density of 1×10^4 cells per well in a 24-well culture plate and cultured overnight in complete medium under standard conditions to allow for full attachment. Subsequently, pGL3-wt-KLF6 or pGL3-mt-KLF6 were co-transfected with miR-455-3p mimics(5′-AUGCAGUCCAUGGGCAUAUACACtt-3′), inhibitor(5′-GUGUAUAUGCCCAUGGACUGCAUtt-3′), or NC(5′-CGUGGGAUCAAACAUCUCCAUGAtt-3′) (GenePharma Co., Ltd, Shanghai, China) into the 293 cells using Lipofectamine 2000 (11,668,019, Thermofisher). The amounts of plasmid DNA and RNA were carefully measured and added according to the instructions provided in the reagent kit. After 48 h, luciferase activity was measured using the Dual Luciferase Reporter Assay System (E1910, WI, USA).

Table 2 Primers information

Name	Sequence (5′-3′)	Application
KLF6-Forward	CTCCGACCCCATTGGCGAAGTTTT	RT-qPCR
KLF6-Reverse	ATGGAGGCGTGGAGGTGACAGAGG	RT-qPCR
Nrf2-Forward	AGCTAGATAGTGCCCCTGGAAGTG	RT-qPCR
Nrf2-Reverse	CTGCCCCTGAGATGGTGACAA	RT-qPCR
β-actin Forward	CCTGTACGCCAACACAGTGC	RT-qPCR
β-actin Reverse	ATACTCCTGCTTGCTGATCC	RT-qPCR
U6 Forward	GTGCTCGCTTCGGCAGCACAT	RT-qPCR
U6 Reverse	TACCTTGCGAAGTGCTTAAAC	RT-qPCR
miR-455-3p Forward	GTGTATATGCCCATGGACTGCAT	RT-qPCR
miR-455-3p Reverse	CAGTGCGTGTCGTGGAGT	RT-qPCR
U6 snRNA RT primer	TACCTTGCGAAGTGCTTAAAC	Reverse transcription
miR-455-3p RT primer	GTCGTATCCAGTGCGTGTCGTGGAGTCGGCAAT TGCACTGGATACGACATGCAG	Reverse transcription
PCR -TFBS-Forward	TTCAGGAGACTGAGGCAGGAGA	ChIP-PCR
PCR -TFBS-Reverse	AGTCTTGCTCTGTCATCCAGGC	ChIP-PCR
miR-455-3p pro-Forward	TTCAGATTATGGATATTAATCATG	Promoter Amplification
miR-455-3p pro-Reverse	GAGACGGAGTCTTGCTCTGTCATCC	Promoter Amplification

Meanwhile, we identified the location of the miR-455-3p precursor in the human genome. Following conventional methods, we selected the region approximately 2.0 kb upstream of the transcription start site as the potential promoter. This core promoter sequence of the miR-455-3p, was predicted using "Promoter 2.0 software" (Technical University of Denmark). Next, "JASPAR" (University of Oslo, Norway; Genome Informatics Lab, UBC; Université Grenoble Alpes, France) was utilized to predict transcription factors with potential transcription factor binding sites (TFBS) within the miR-455-3p promoter. Upon completing the above work, the miR-455-3p promoter was amplified using human genomic DNA as the template, with the PCR primer details provided in Table 2. The amplified product was used to construct pGL3-pro-miR-455-3p-TFBS(wt), which contains a reporter gene expression system composed of the miR-455-3p promoter and the luciferase gene. Then the TFBS was subsequently mutated to create pGL3-pro-miR-455-3p-TFBS(mt). At the same time, a recombinant plasmid, pcDNA-Nrf2, for overexpressing Nrf2 was constructed. Next, pGL3-pro-miR-455-3p-TFBS(wt) or pGL3-pro-miR-455-3p-TFBS(mt) was co-transfected with pcDNA-Nrf2 into 293 cells. Forty-eight h post-transfection, luciferase activity was measured to determine whether Nrf2 binds to the predicted TFBS on the miR-455-3p promoter and regulates its transcription.

2.6 Chromatin immunoprecipitation-PCR (ChIP-PCR)

AGS cells were transfected with pcDNA-HA-Nrf2 for 72 h. Following transfection, the cells were harvested and processed for ChIP using the EZ ChIP Kit (Millipore, MI, USA) according to the manufacturer's protocol. To immunoprecipitate the target protein, 4 µg of anti-HA tag primary antibody (ab236632, Abcam) was used. For western blotting, an 11% separating gel was utilized. The primary antibody was diluted to 1:600, and the HRP-conjugated goat anti-rabbit secondary antibody (sc-2004, 1:3000, Santa Cruz, CA, USA) was applied. A hypothetical 103 bp fragment containing the Nrf2 TFBS will be identified by performing 2% agarose gel electrophoresis on the PCR products amplified using DNA extracted from the HA-Nrf2 protein elution as a template. Primers used for PCR are provided in Table 2.

2.7 Evaluation of the effects of TB-II on Nrf2 protein synthesis, degradation, and autophagy in GC cells

AGS cells in the logarithmic growth phase were seeded into 6-well culture plates at a density of 1×10^5 cells per well. The cells were cultured overnight under normal conditions in complete medium until they adhered completely. After adhesion, the cells were divided into five groups: (1) Control group (no treatment). (2) TB-II group (Cells were treated with 5 µg/ml TB-II for 48 h). (3) Cycloheximide (CHX)+TB-II group (Cells were co-treated with 50 µg/ml CHX and 5 µg/ml TB-II for 48 h). (4) Bortezomib+TB-II group (Cells were co-treated with 50 nM bortezomib and 5 µg/ml TB-II for 48 h). (5) Chloroquine + TB-II group (Cells were co-treated with 20 µM Chloroquine and 5 µg/ml TB-II for 48 h). CHX, Bortezomib,

and Chloroquine were purchased from Sigma-Aldrich. After treatment, the cells were harvested, and western blotting was performed to assess Nrf2 protein levels.

2.8 Investigation of the effects of TB-II on Keap1 protein expression and downstream Nrf2-regulated genes (Cyclin D1, MMP9, and E-cadherin) in GC cells

AGS cells in the logarithmic growth phase were seeded into 6-well culture plates at a density of 1×10^5 cells per well. The cells were then incubated overnight under standard conditions in complete medium to allow full adhesion. After adhesion, the cells were divided into five groups: (1) Control group (no treatment). (2) TB-II group (Cells were treated with 5 μg/ml TB-II for 48 h). (3) SiRNA-Keap1+TB-II group (Cells were transfected with siRNA targeting Keap1 and then treated with 5 μg/ml TB-II for 48 h). (4) SiRNA-KLF6+TB-II group (Cells were transfected with siRNA targeting KLF6 and then treated with 5 μg/ml TB-II for 48 h). (5) SiRNA-NC+TB-II group (cells were transfected with a siRNA-NC and then treated with 5 μg/ml TB-II for 48 h). SiRNA transfection was performed 24 h prior to TB-II treatment, following the manufacturer's instructions for Lipofectamine2000. The siRNA-KLF6(5′-GUUUACCUCCGACCCCAUU-3′), siRNA-Keap1(5′-GUACGACUGCGA ACAGCGA-3′), and siRNA-NC (5′-CGUCUCCAUUACUCAGUCC-3′) were synthesized by Shanghai GenePharma Co., Ltd. and diluted to 100 mM using DEPC-treated water for transfection. Following TB-II treatment, cells from both the control and TB-II groups were h collected for total protein extraction, and western blotting was conducted to evaluate Keap1 protein expression. Additionally, total RNA was extracted from all groups and utilized for RT-qPCR to quantify the mRNA levels of CyclinD1, MMP9, and E-cadherin.

2.9 Immunoprecipitation assay

NCI-N87 cells, pre-transfected with the pcDNA-HA-Keap1, were reseeded into 6-well culture plates at a density of 1×10^5 cells per well. The cells were cultured overnight under standard conditions to allow full adherence and were then divided into two groups: (1) Control group (no treatment). (2) TB-II group (Cells were treated with 5 μg/ml TB-II for 48 h). After treatment, total proteins were extracted, and immunoprecipitation was performed to isolate HA-tagged Keap1 using 5 μg of rabbit polyclonal to HA tag (Abcam). Subsequently, western blotting was conducted to detect the binding of Nrf2 protein. For western blotting, an 11% separating gel was used. The primary antibodies were diluted as follows: anti-Keap1 (1:800) and anti-Nrf2 (1:600). The secondary antibody was an HRP-conjugated goat anti-rabbit antibody (1:3000).

2.10 RT-qPCR

Total RNA was extracted and reverse-transcribed into cDNA using M-MLV reverse transcriptase. RT-qPCR was conducted with the SYBR Premix Ex Taq kit on the ABI7500 Fast system (Thermo Fisher Scientific). Gene expression levels of KLF6, Nrf2, and miR-455-3p were normalized to their respective internal controls (β-actin for KLF6 and Nrf2; U6 snRNA for miR-455-3p), with relative expression calculated using the $2^{-\Delta\Delta Ct}$ method. Specific primers for U6 snRNA and miR-455-3p were used for both reverse transcription and RT-qPCR (Table 2). Thermal cycling conditions included an initial denaturation at 95 °C for 10 s, followed by 40 cycles of 95 °C for 10 s, 60 °C for 20 s, and 72 °C for 20 s.

2.11 Western blot

Total protein was extracted using the M-PER Mammalian Protein Extraction Reagent (Thermofisher), and protein concentrations were measured via the BCA assay. Equal amounts of protein (12 μg) were separated on the 11–12% SDS-PAGE gel, transferred to nitrocellulose membranes, and blocked with 5% non-fat milk in TBST for 1 h at room temperature. Membranes were briefly stained with Ponceau S to verify target bands and compared with pre-stained molecular weight markers. They were then incubated overnight at 4 °C with primary antibodies against Keap1(1:300), Nrf2 (1:600), KLF6 (1:500), and β-actin (1:1000) (Abcam/Santa Cruz). After washing, membranes were incubated for 2 h at room temperature with HRP-conjugated goat anti-mouse or anti-rabbit secondary antibodies (1:3000, Santa Cruz). Protein bands were visualized using ECL and imaged on X-ray films, with β-actin serving as a loading control for normalization.

2.12 Statistical analysis

All data are presented as the mean ± standard deviation (SD) from three independent experiments. Statistical analyses were conducted using SPSS GradPack version 20.0 (IBM Corp., Armonk, NY, USA) and GraphPad Prism 7.0 (GraphPad Software, Inc., La Jolla, CA, USA). Group comparisons were evaluated using either a two-tailed Student's *t*-test or one-way analysis of variance (ANOVA) followed by Tukey's post-hoc test for multiple comparisons. A *p*-value of less than 0.05 was considered to indicate statistical significance.

3 Results

3.1 Reduced KLF6 protein expression links to higher tumor malignancy and inverse miR-455-3p levels in GC stage I to III

RT-qPCR and ELISA results showed significantly lower KLF6 mRNA and protein expression in GC tissues than in adjacent tissues ($p < 0.01$), regardless of stage I or III. No significant difference was found in KLF6 mRNA levels between stage I and III ($p > 0.05$), but protein expression was significantly lower in stage III than in stage I ($p < 0.01$). Adjacent tissues from both stages showed no significant differences in KLF6 mRNA or protein expression ($p > 0.05$) (Fig. 1A, B). Further analysis revealed no significant variation in KLF6 mRNA levels among stage I, II, and III GC samples. However, KLF6 protein expression showed a progressive decline with tumor stage ($p < 0.05$ for Stage III vs. Stage II and Stage II vs. Stage I; $p < 0.01$ for Stage III vs. Stage I) (Fig. 1C, D). RT-qPCR results indicated a stage-dependent increase in miR-455-3p levels ($p < 0.05$ for Stage III vs. Stage II and Stage II vs. Stage I; $p < 0.01$ for Stage III vs. Stage I) (Fig. 1E). A negative correlation was observed between KLF6 protein expression and miR-455-3p levels across all GC stages (Fig. 1F).

3.2 TB-II treatment effectively inhibits proliferation and induces apoptosis in GC cells

The CCK-8 assay results showed that TB-II (LD and HD) effectively inhibited the logarithmic proliferation of AGS and NCI-N87 cells ($p < 0.05$ or 0.01 vs. control group, 72 h), with HD exerting a stronger effect ($p < 0.01$ vs. LD-TB-II group). However, the proliferation was significantly increased in the Lv-shRNA-KLF6 + HD-TB-II group compared to the HD-TB-II group ($p < 0.01$, 72 h) (Fig. 2A). TUNEL staining confirmed that TB-II induced apoptosis in both cell lines after 48 h ($p < 0.05$ or 0.01 vs. control group), with HD-TB-II promoting apoptosis more effectively ($p < 0.01$, vs. LD-TB-II). Notably, apoptosis was significantly reduced in the Lv-shRNA-KLF6 + HD-TB-II group compared to the HD-TB-II group($p < 0.01$) (Fig. 2B, C).

3.3 TB-II upregulates Nrf2 protein and miR-455-3p expression while downregulating KLF6 protein expression in GC cells

The RT-qPCR results indicated that compared to the control group, miR-455-3p levels were significantly reduced in GC cells in the LD-TB-II group ($p < 0.05$ or 0.01). Furthermore, the decrease in miR-455-3p levels was more pronounced in the HD-TB-II group ($p < 0.01$, vs. control or LD-TB-II groups) (Fig. 3A). Western blotting analysis revealed that the expression trend of Nrf2 protein in both AGS and NCI-N87 cells across all groups mirrored the changes observed in miR-455-3p levels, whereas KLF6 exhibited an entirely opposite trend to that of miR-455-3p (Fig. 3B, C).

3.4 MiR-455-3p suppresses KLF6 by targeting Its 3′-UTR

Bioinformatics analysis identified an 8-base miR-455-3p binding site, 5′-GGACUGCA-3′, in the 3′-UTR of human KLF6 mRNA (Fig. 4A). Luciferase assay results demonstrated that both pGL3-wt-KLF6 and pGL3-mt-KLF6 transfected 293 cells had significantly higher luciferase activity than the control group (p all < 0.01). Compared to pGL3-wt-KLF6 group, luciferase activity was significantly reduced by miR-455-3p mimics ($p < 0.01$) and increased by the miR-455-3p inhibitor ($p < 0.05$),

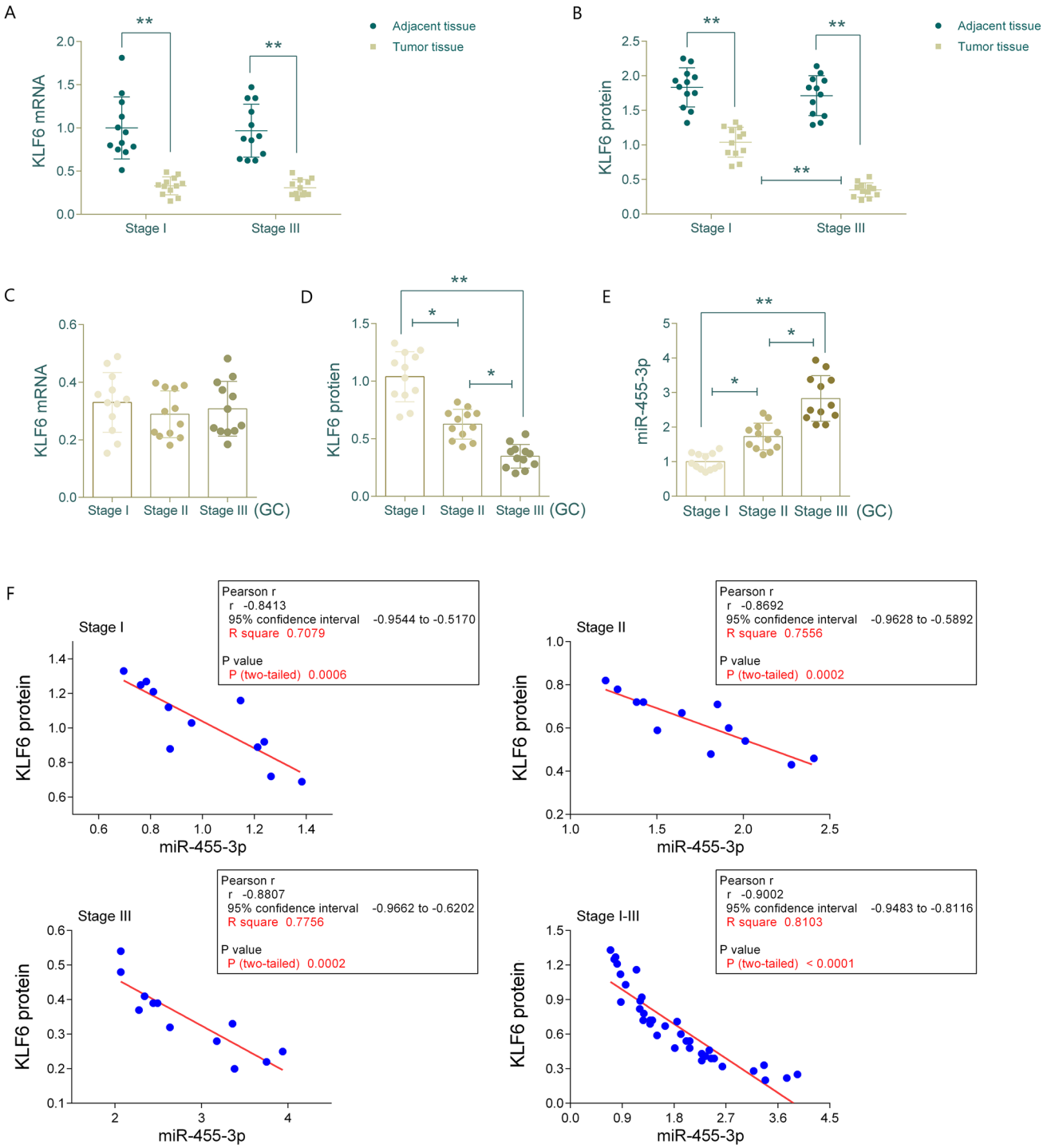

Fig. 1 Analysis of KLF6 and miR-455-3p Expression and Their Correlation in Grade I-III GC Tissues. **A** KLF6 mRNA levels in Grade I/III GC tissues and adjacent tissues were measured by RT-qPCR. **B** KLF6 protein levels (ng protein/g tissue) in Grade I/III GC tissues and adjacent tissues were assessed by ELISA. **C** KLF6 mRNA levels in GC tissues at stages I-III were measured by RT-qPCR. **D** KLF6 protein levels (ng protein/g tissue) in GC tissues at stages I-III were evaluated by ELISA. **E** MiR-455-3p levels in GC tissues at stages I-III were determined by RT-qPCR. **F** Correlation analysis. For RT-qPCR, β-actin and U6 were used as internal controls, and inter-group differences were analyzed using the $2^{-\Delta\Delta Ct}$ method. Data are presented as the mean ± SD. The protein and mRNA levels are both expressed as fold changes relative to the control group. Sample size: n = 12. $^{**}p < 0.01$, $^{*}p < 0.05$

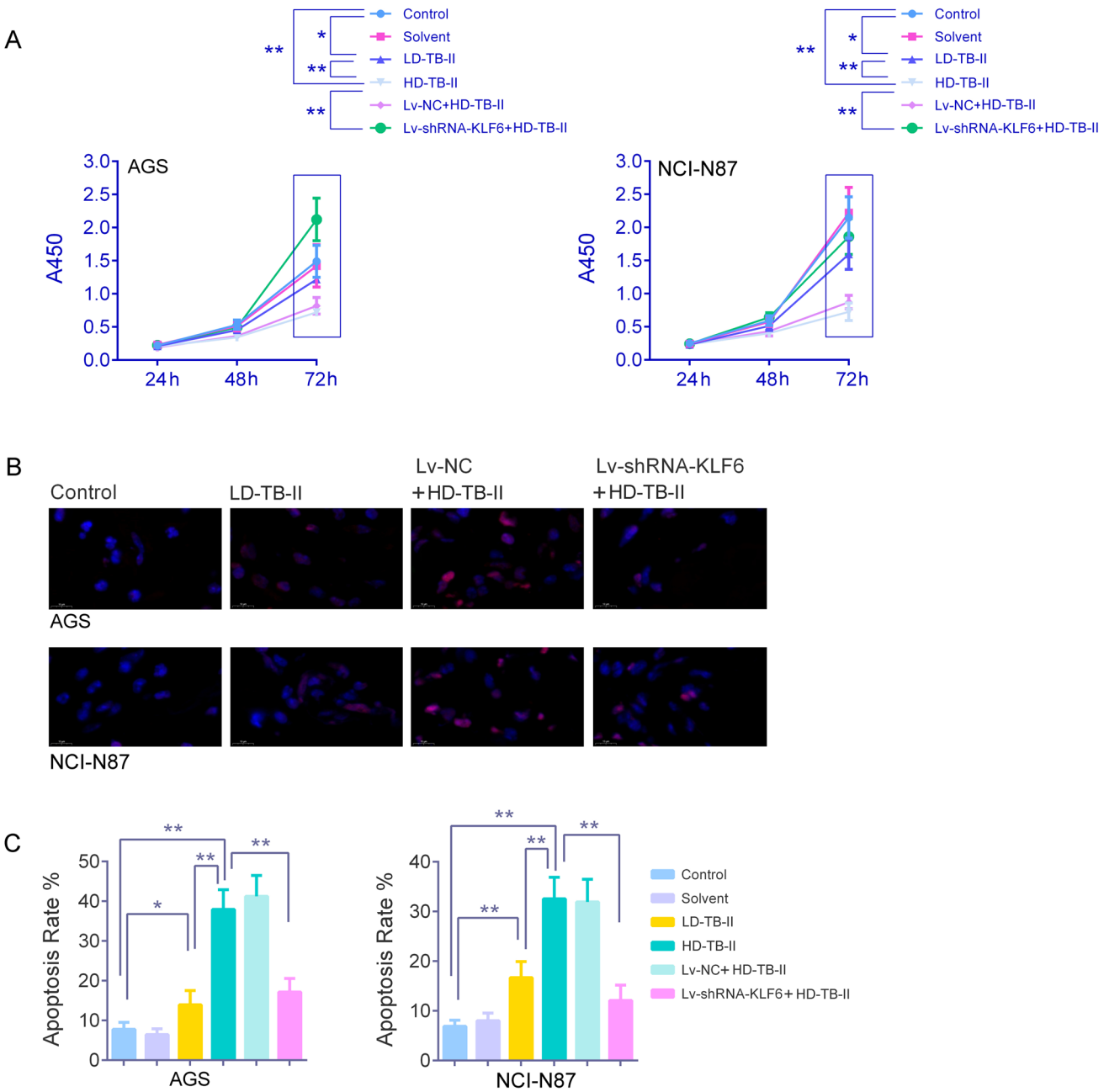

Fig. 2 Proliferation Assay and TUNEL Staining. **A** Cell proliferation of AGS and NCI-N87 cells following TB-II treatment was assessed using the CCK-8 assay. The x-axis represents different experimental groups, and the y-axis indicates the absorbance at 450 nm. **B**, **C** TUNEL Staining was performed to detect apoptotic cells. The magnification of the cells was 200×. To objectively assess the differences in apoptosis rates between groups, 5 random fields were selected per sample for counting apoptotic cells. The assay was conducted in biological triplicates (n = 3), and the data are presented as the mean ± SD. $^{**}p < 0.01$, $^{*}p < 0.05$

with no change in the pGL3-wt-KLF6 + miR-455-3p NC group ($p > 0.05$). In contrast, luciferase activity remained unchanged across all groups in the pGL3-mt-KLF6 transfected cells ($p > 0.05$) (Fig. 4B).

3.5 Nrf2 binds to the miR-455-3p promoter and activates transcription

Bioinformatics analysis identified a 574 bp miR-455-3p promoter containing a conserved Nrf2 binding site (5′-TGACAGAGCA-3′) (Fig. 4C). Luciferase assays demonstrated that Nrf2 overexpression significantly increased luciferase activity in pGL3-pro-miR-455-3p-TFBS(wt) transfected 293 cells ($p < 0.01$), but had no effect on pGL3-pro-miR-455-3p-TFBS(mt) transfected cells

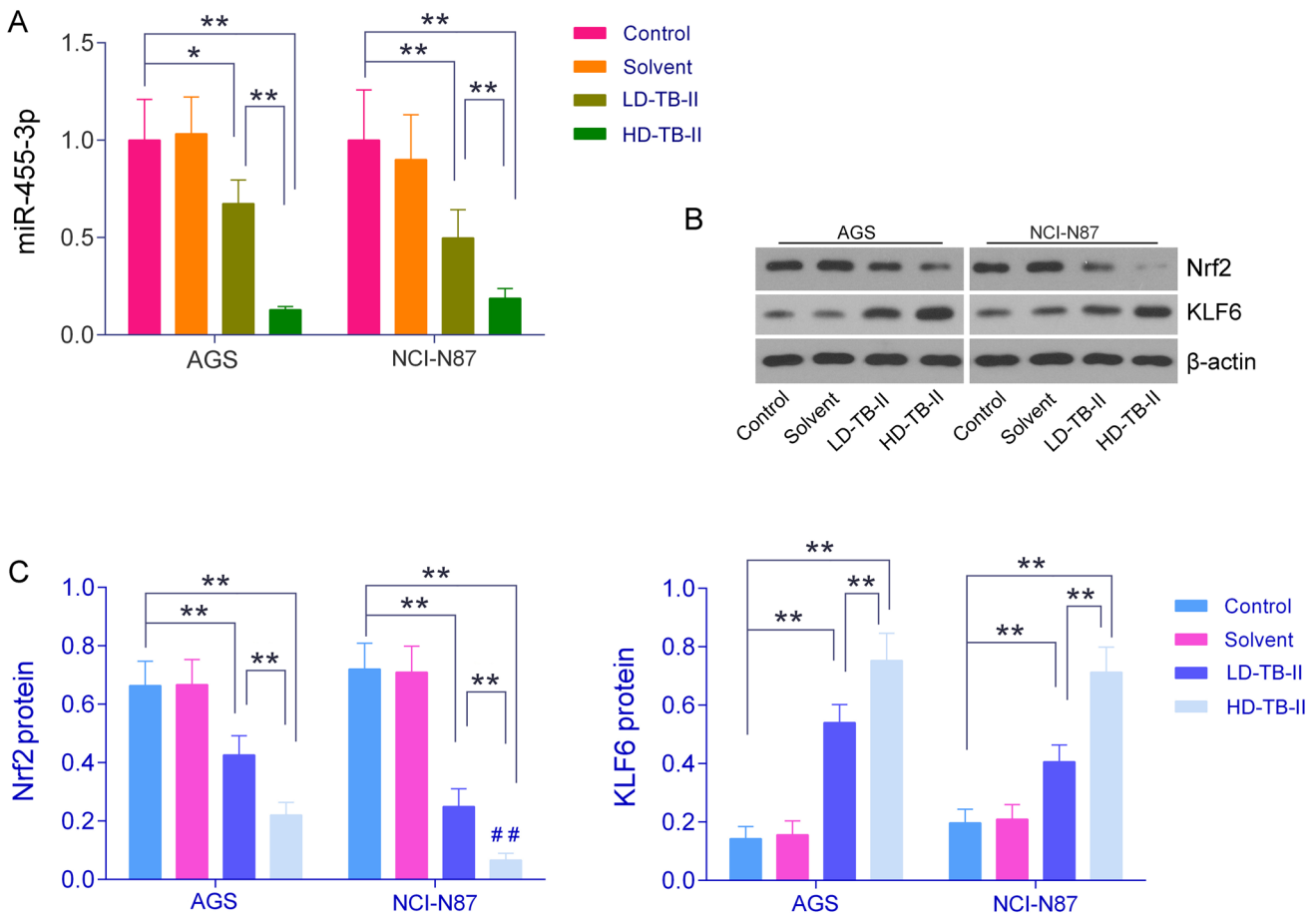

Fig. 3 Detection of Nrf2, Keap1, and miR-455-3p Expression in GC Cells Under TB-II Treatment Conditions. **A** Detection of miR-455-3p content in GC cells of each group by RT-qPCR. U6 were used as internal controls. **B**, **C** Detection of Nrf2 and KLF6 protein expression in GC cells of each group by western blotting. β-actin was used as the loading control. The tests were carried out on three biological replicates(n = 3), and the data are expressed as the mean ± SD. ** $p < 0.01$, * $p < 0.05$

($p > 0.05$), confirming that Nrf2 activates miR-455-3p transcription by binding to its promoter (Fig. 4D). ChIP-PCR further confirmed that the TFBS-containing promoter region was enriched in Nrf2-bound DNA from AGS cells transfected with pcDNA-HA-Nrf2 (Fig. 4E).

3.6 TB-II inhibits Nrf2 activity by upregulation keap1 expression

Western blot analysis demonstrated that treatment with 5 μg/ml TB-II for 48 h effectively inhibited Nrf2 protein expression in AGS cells ($p < 0.05$, vs control group). Nrf2 levels were further reduced in the CHX (50 μg/ml) + TB-II group but increased in the 50 nM Bortezomib + TB-II group ($p < 0.01$, vs. TB-II group). However, Chloroquine (20 μM) had no significant effect on Nrf2 protein in TB-II treated AGS cells ($p > 0.05$) (Fig. 5A). Further western blot analysis confirmed that TB-II (5 μg/ml, 48 h) significantly upregulated Keap1 expression (Fig. 5B). Immunoprecipitation demonstrated that TB-II enhanced the Nrf2-Keap1 interaction in AGS cells (Fig. 5C). RT-qPCR analysis revealed that TB-II downregulated CyclinD1 and MMP9 mRNA levels while upregulating E-cadherin ($p < 0.01$, *vs.* control group). Keap1 or KLF6 silencing reversed these effects ($p < 0.01$ vs. TB-II group) (Fig. 5D).

4 Discussion

Timosaponin, a natural compound from *Anemarrhena asphodeloides*, has gained attention for its antitumor properties. It inhibits the proliferation of various cancer cells, including those of the stomach, breast, and liver. Among its forms, Timosaponin-AIII (TA-III), a steroidal saponin, exhibits potent anticancer activity, particularly in breast, liver, and lung

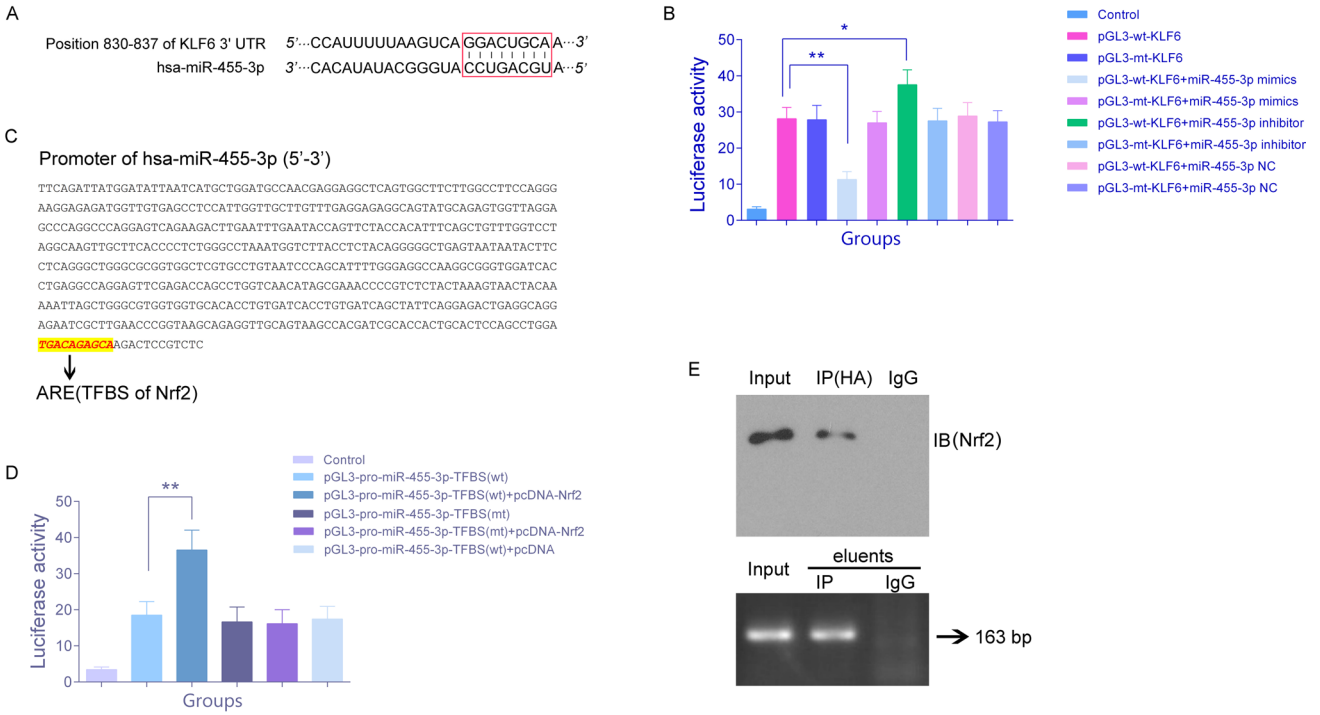

Fig. 4 Luciferase assay and ChIP-PCR. **A**Verification of the binding sites of miR-455-3p within the 3′-UTR of KLF6 mRNA. **B** Measurement of firefly luciferase activity 48 h post-transfection in 293 cells from each group, with statistical analysis of differences. The histogram illustrates the relative firefly luciferase activity across the groups. **C** Verification of the Nrf2 TFBS in the miR-455-3p promoter. **D** Comparison of luciferase activity differences between the groups. The x-axis represents the transfection groups, and the y-axis shows the relative luciferase activity. Renilla luciferase was used as the internal control for the relative luciferase assay. **E** ChIP-PCR assay. Immunoprecipitation of HA-Nrf2 (Upper panel), PCR amplification of the predicted Nrf2 binding DNA in the miR-455-3p promoter, followed by 2% gel electrophoresis of the PCR products (Lower panel). The tests were conducted in triplicate biological replicates (n = 3), and data are expressed as the mean ± SD. $^{**}p < 0.01$, $^{*}p < 0.05$

cancers. TA-III binds to HSP90, promoting GPX4 degradation and leading to iron accumulation and ferroptosis in non-small cell lung cancer (NSCLC) cells [6]. Research by Okkeun Jung et al. shows that TA-III suppresses NSCLC A549 cell migration and invasion by inhibiting the ERK1/2, Src/FAK, and β-catenin pathways, leading to MMP-2 and MMP-9 down-regulation, highlighting its potential as a therapeutic candidate for NSCLC [6, 8]. Beyond its direct anticancer effects, Timosaponin possesses antioxidant and anti-inflammatory properties, reducing oxidative stress and inflammation within the tumor microenvironment. It also modulates various signaling pathways, impacting tumor growth and progression. In colorectal cancer (CRC), TA-III induces lipophagy via the Rab7 gene, promoting ferroptosis, further supporting its potential as an anticancer agent [9]. Despite TA-III's potent anticancer effects, its clinical application is hindered by low bioavailability, poor solubility, weak targeting, and potential toxicity. This highlights the need to explore other active anticancer components of Timosaponin with improved targeting, specificity, and safety. While most research focuses on TA-III, identifying additional bioactive components remains crucial for advancing cancer therapy. Collectively, these studies underscore Timosaponin's potential as a promising anticancer agent, warranting further investigation and development.

The KLF (Kruppel-like factor) gene family regulates transcription in mammals and is crucial for cell differentiation, proliferation, and angiogenesis [10]. Among them, KLF6, also known as zinc finger transcription factor 9 (ZF9) or core promoter element binding protein (CPBP), is located on human chromosome 10p15 and spans approximately 7 kb. Initially identified in a placental gene expression library, KLF6 functions as a nuclear transcription regulator, it plays a key role in regulating genes contributing to cell differentiation, development, and growth signal transduction, essential for both normal tissue development and the initiation and tumor progression [11]. Recent studies link KLF6 gene mutations to multiple cancers, including prostate, breast, NSCLC, liver, and colorectal cancers. Tumorigenesis often involves KLF6 deletions, point mutations, or promoter methylation [12–14]. In GC, Jaya Sangodkar et al. identified KLF6 deletions in 53% of GC samples, with four missense mutations (T179I, R198G, R71Q, and S180L), suggesting wild-type KLF6 (wtKLF6) loss correlates with tumor progression. Further studies confirmed that wtKLF6 suppresses GC cell proliferation by regulating p21 and C-myc. These findings establish KLF6 as a tumor suppressor in GC [15–17]. However, as of now, there are no

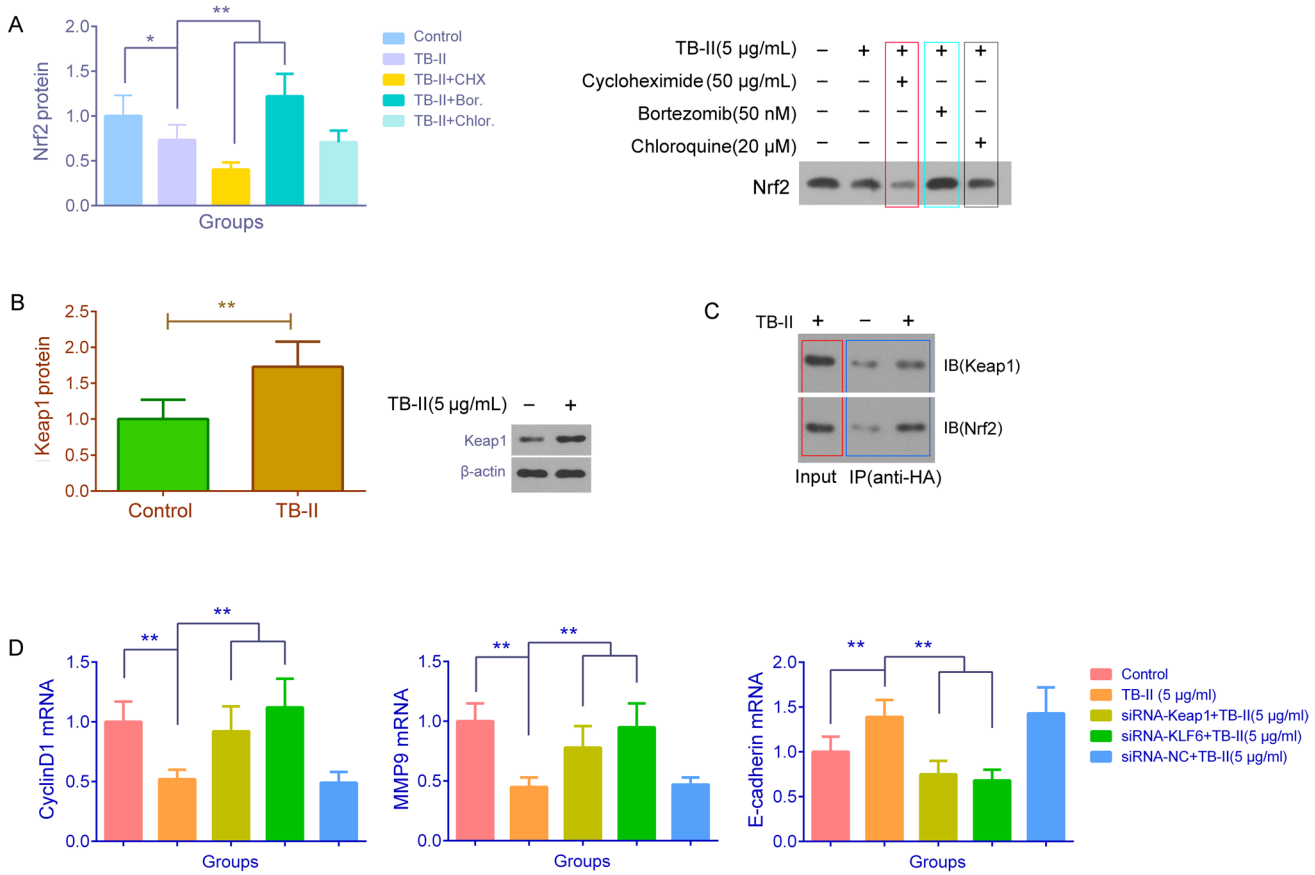

Fig. 5 Detection of TB-II Treatment Effects on Nrf2 Protein Synthesis and Degradation, Keap1 Expression, Keap1/Nrf2 Complex Formation, and Nrf2 Downstream Gene Transcription in GC Cells. **A** Western blot analysis was performed to assess Nrf2 protein expression in AGS cells after 48 h of TB-II treatment. Cycloheximide, Bortezomib, and Chloroquine were added 1 h before TB-II treatment. **B** Western blot was conducted to measure Keap1 protein expression in AGS cells treated with 5 μg/ml TB-II for 48 h. **C** Immunoprecipitation assays were conducted to detect the Keap1/Nrf2 complex in AGS cells, both treated and untreated with 5 μg/ml TB-II for 48 h. **D** RT-qPCR was used to measure the mRNA levels of CyclinD1, MMP9, and E-cadherin in AGS cells from different treatment groups. β-actin was used as the loading and internal control in western blotting and RT-qPCR, respectively. Inter-group differences were analyzed using the $2^{-\Delta\Delta Ct}$ method. The protein and mRNA levels are expressed as fold changes relative to the control group. All experiments were performed in triplicate (n = 3), and data are presented as the mean ± SD. ** $p < 0.01$, * $p < 0.05$

reported studies on the active components of natural compounds driving KLF6 expression to regulate the progression of GC or other malignant tumors. While KLF6 is recognized as a tumor suppressor involved in various cancers, its direct regulation by natural compounds remains unexplored. Given KLF6's critical role in cell proliferation, differentiation, and apoptosis, further investigation into whether natural bioactive compounds can modulate KLF6 expression and influence tumor progression is warranted. This area of research holds potential for discovering novel therapeutic strategies and should be given more attention in future studies. Our research revealed that KLF6 undergoes post-transcriptional suppression during GC progression, significantly limiting its tumor-suppressive function. This finding suggests that restoring KLF6 expression could be a promising strategy for inhibiting GC progression. Encouragingly, we identified TB-II as an effective agent in reversing this suppression, a conclusion supported by experiments demonstrating its inhibitory effects on proliferation and invasion in GC cells.

Research has shown that oxidative stress plays a crucial role in GC by affecting key effector proteins. Nrf2, a transcription factor, regulates antioxidant enzymes like glutathione S-transferase and NAD(P)H quinone dehydrogenase 1 (NQO1) through antioxidant response elements (AREs). Persistent Nrf2 activation is linked t to poor prognosis in cancers such as bladder and lung cancer. In 2021, Lv J et al. identified the Nestin-Keap1-Nrf2 axis as essential for GC cell proliferation and migration by combating oxidative stress [18]. Similarly, Da Zhi Fu et al. found that ATF3 sensitizes GC cells to cisplatin by blocking Nrf2/Keap1/XCT signaling, inducing ferroptosis, and potentially overcoming chemoresistance. Although Nrf2 regulates antioxidant genes, its exact role in GC remains unclear [19]. In our study, we first identified an ARE element in the

promoter region of miR-455-3p, and found that Nrf2 can positively regulate the transcription of miR-455-3p by binding to ARE. The uncontrolled activation of Nrf2 in malignancies enhances antioxidant capacity, promotes chemoresistance, and correlates with poor prognosis. Targeting Nrf2 through inhibitors or redox balance regulation is a promising approach for GC treatment. In this study, we confirmed the actual existence of the Nrf2/miR-455-3p/KLF6 regulatory pathway in GC progression, the upregulation of KLF6 expression by TB-II in GC cells depends on its inhibition of Nrf2 activity.

Keap1, a negative regulator of Nrf2, plays a crucial role in controlling antioxidant gene expression. In the cytoplasm, Keap1 binds to Nrf2, facilitating its ubiquitination and degradation, thereby preventing excessive activation of ARE under normal conditions. Given its essential role in Nrf2 regulation, Keap1 has emerged as a promising therapeutic target for inhibiting Nrf2 activity, targeting Keap1 provides a potential approach for modulating redox balance and combating Nrf2-driven tumor progression [20, 21]. Our study confirms that TB-II inhibits Nrf2 activity by upregulating Keap1 expression. We observed that TB-II suppresses Nrf2 protein expression in GC cells without affecting its mRNA levels. It also showed a synergistic effect with CHX, while bortezomib reversed its inhibition, indicating that TB-II promotes Nrf2 degradation via the proteasome. However, chloroquine had no effect when combined with TB-II, suggesting that autophagy is not involved, and Nrf2 degradation is ubiquitin-dependent. Since Keap1 regulates Nrf2 through ubiquitination, we propose that TB-II indirectly modulates Nrf2 via Keap1. Indeed, 5 μg/ml of TB-II significantly increased Keap1 protein levels and enhanced Keap1-Nrf2 complex formation. These findings explain TB-II's effect on Nrf2 and support the role of Keap1 in binding Nrf2, preventing its nuclear translocation, and facilitating its degradation.

Currently, research on the role of miR-455-3p in GC remains limited but is gaining increasing attention. While multiple studies consistently report that miR-455-3p expression is significantly lower in GC cells than in normal gastric epithelial cells and that its upregulation suppresses GC cell proliferation and promotes apoptosis, its precise mechanism of action remains incompletely understood [22, 23]. As a tumor suppressor gene, KLF6 is regulated by multiple miRNAs in various cancers. However, direct evidence linking miR-455-3p to KLF6 in GC progression remains scarce, and research in this area is still at an exploratory stage. In our study, we observed a progressive decrease in KLF6 expression as GC advanced, driven by post-transcriptional mechanisms. This suggests the involvement of key upstream miRNAs in regulating KLF6

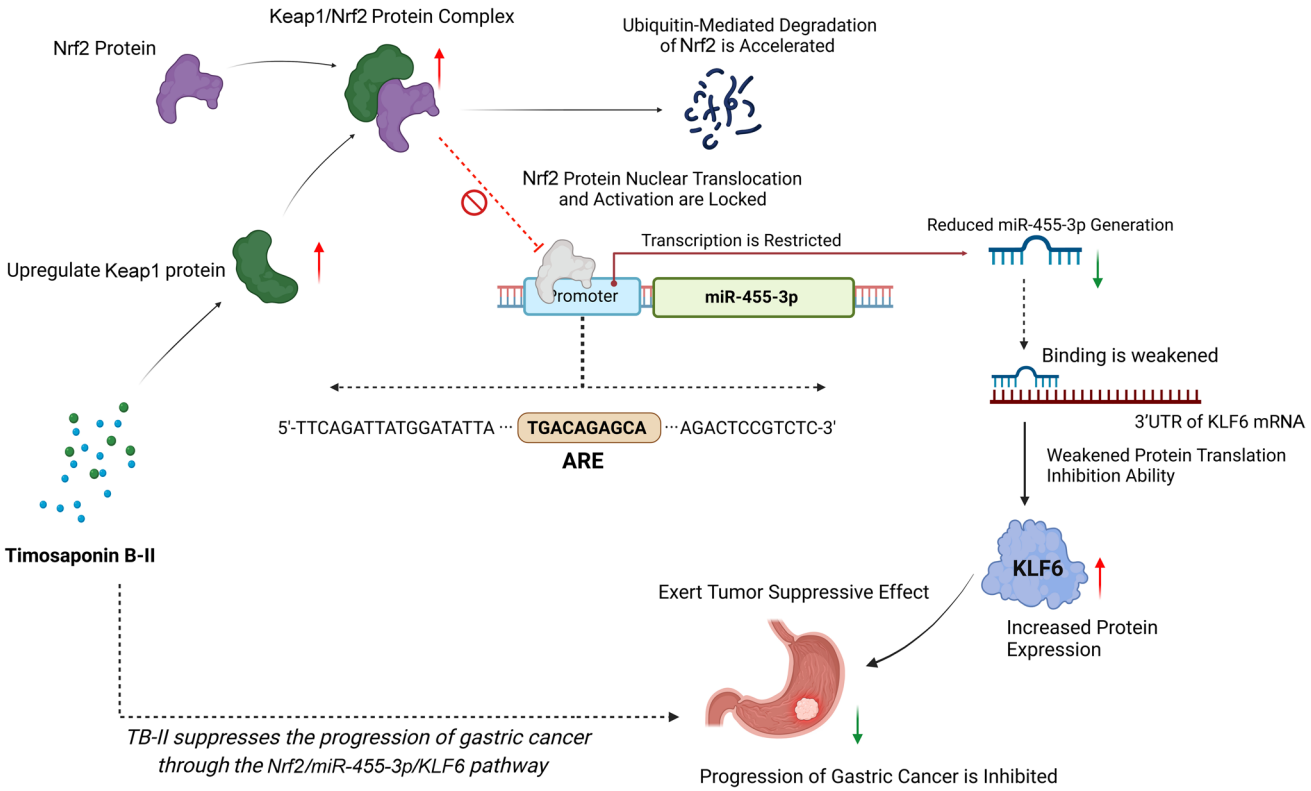

Fig. 6 Molecular Mechanism of TB-II Inhibiting GC Cells Proliferation and Inducing Apoptosis via the Nrf2/miR-455-3p/KLF6 Pathway

expression. To identify these regulatory miRNAs, we conducted bioinformatics analyses, luciferase reporter assays, and other molecular studies, ultimately confirming miR-455-3p as a key player. The significance of screening miR-455-3p lies in its role in refining the pathway through which TB-II inhibits GC progression. It mediates the impact of TB-II on the tumor suppressor gene KLF6 via its target Keap1. This discovery not only enhances our understanding of miR-455-3p's function within the GC regulatory network but also offers a novel perspective for exploring the anticancer mechanisms of natural compounds through miRNA-mediated regulation. Our study offers a preliminary insight into the mechanism by which TB-II inhibits the progression of GC, highlighting the pivotal role of the Nrf2/miR-455-3p/KLF6 pathway in mediating TB-II's anticancer effects. These findings provide a theoretical foundation for the potential application of TB-II and its related compounds in the prevention and treatment of GC, as well as other malignant tumors. In addition, our results suggest that Keap1 mediates the effects of TB-II on the Nrf2/miR-455-3p/KLF6 pathway, positioning it as a potential target for the development of more effective anticancer derivatives based on TB-II for the future prevention and treatment of GC.

While the conclusions of this study are compelling, there are still some limitations, and several unresolved questions remain that require further investigation. First, it is essential to investigate the interaction between Keap1 and TB-II in greater depth using advanced techniques. A comprehensive study should be conducted utilizing surface plasmon resonance (SPR), drug affinity responsive target stability (DARTS), and bioinformatics docking, which are crucial for solidifying Keap1 as a target for TB-II's anti-gastric cancer effects. Additionally, this study has only verified in vitro that TB-II inhibits GC cell proliferation and induces apoptosis through the Nrf2/miR-455-3p/KLF6 pathway. However, long-term in vivo validation of these mechanisms is necessary. In the future, we plan to establish subcutaneous GC xenograft models, spleen-liver metastasis models, and patient-derived xenograft (PDX) models to validate TB-II's inhibitory effect on GC progression and its underlying mechanisms from multiple perspectives. Furthermore, confirming Keap1 as a drug target through Keap1 gene knockout experiments will be an indispensable part of the research.

In conclusion, our study demonstrates that TB-II inhibits GC cell proliferation and promotes apoptosis by modulating the Nrf2/miR-455-3p/KLF6 pathway through Keap1 (the schematic of the mechanism is shown in Fig. 6), supporting its potential for GC treatment.

Acknowledgements None.

Author contributions Conceptualization, Qiaoyan Cui and Yan Qiu; Funding acquisition, Xuesong Bai and Yan Qiu; Methodology, Qiaoyan Cui and Ruijie Zhang; Investigation, Qiaoyan Cui, Shiqiao Zhao, Jian Wang, Yafen Dong and Xuesong Bai; Validation, Xuesong Bai and Ye Chen; Supervision, Shiqiao Zhao and Ye Chen; Project Administration, Qiaoyan Cui and Yan Qiu; Data Curation and Qiaoyan Cui; Writing-original draft, Shiqiao Zhao and Yan Qiu. Preparation of Figures, Qiaoyan Cui and Ruijie Zhang. All authors reviewed the manuscript.

Funding This study was supported by the Medical Discipline Construction Program of Shanghai Pudong New Area Health Commission (the Key Weak Disciplines Program) (Grant No. PWZbr2022-13), the Outstanding Leaders Training Program of Shanghai Pudong New Area Health Commission (Grant No. PWRI 2020-08) and the Young Medical Talents Training Program of Shanghai Pudong New Area Health Commission (PWRq2024-44).

Data availability All data generated or analysed during this study are included in this published article.

Declarations

Ethics approval and consent to participate This study was approved by the Ethics Committee of Shanghai Pudong New Area People's Hospital (Approval Number: 2023-LW-09).

Consent for publication All authors have read and agreed with the content of the manuscript.

Competing interests The authors declare no competing interests.

References

1. Okuno K, Tokunaga M, Yamashita Y, Umebayashi Y, Saito T, Fukuyo R, Sato Y, Saito K, Fujiwara N, Hoshino A, Kawada K, Matsuyama T, Kinugasa Y. Impact of preoperative time interval on survival in patients with gastric cancer. World J Surg. 2021;45(9):2860–7. https://doi.org/10.1007/s00268-021-06187-0.
2. Milano AF. 20-year comparative survival and mortality of cancer of the stomach by age, sex, race, stage, grade, cohort entry time-period, disease duration and selected ICD-O-3 oncologic phenotypes: a systematic review of 157,258 cases for diagnosis years 1973-2014. J Insur Med. 2019;48(1):5–23. https://doi.org/10.17849/insm-48-1-1-19.1.
3. Furukawa K, Irino T, Makuuchi R, Koseki Y, Nakamura K, Waki Y, Fujiya K, Omori H, Tanizawa Y, Bando E, Kawamura T, Terashima M. Impact of preoperative wait time on survival in patients with clinical stage II/III gastric cancer. Gastric Cancer. 2019;22(4):864–72. https://doi.org/10.1007/s10120-018-00910-y.
4. Newman DJ, Cragg GM. Natural products as sources of new drugs from 1981 to 2014. J Nat Prod. 2016;29(6):629. https://doi.org/10.1021/acs.jnatprod.5b01055.
5. Bai Z, Yao C, Zhu J, Xie Y, Ye X-Y, Bai R, Xie T. Anti-tumor drug discovery based on natural product β-elemene: anti-tumor mechanisms and structural modification. Molecules. 2021;26(6):1499. https://doi.org/10.3390/molecules26061499.
6. Zhou C, Yu T, Zhu R, Lu J, Ouyang X, Zhang Z, Chen Q, Li J, Cui J, Jiang F, Jin KY, Sarapultsev A, Li F, Zhang G, Luo S, Hu D. Timosaponin AIII promotes non-small-cell lung cancer ferroptosis through targeting and facilitating HSP90 mediated GPX4 ubiquitination and degradation. Int J Biol Sci. 2023;19(5):1471–89. https://doi.org/10.7150/ijbs.77979.
7. Tu H, Zhou X, Zhou H, Luo Z, Yan Y, Luo Z, Qi Q. Anti-tumor effect and mechanisms of Timosaponin AIII across diverse cancer progression. Biochem Pharmacol. 2024. https://doi.org/10.1016/j.bcp.2024.116080.
8. Jung O, Lee J, Lee YJ, Yun JM, Son YJ, Cho JY, Ryou C, Lee SY. Timosaponin AIII inhibits migration and invasion of A549 human non-small-cell lung cancer cells via attenuations of MMP-2 and MMP-9 by inhibitions of ERK1/2, Src/FAK and β-catenin signaling pathways. Bioorg Med Chem Lett. 2016;26(16):3963–7. https://doi.org/10.1016/j.bmcl.2016.07.004.
9. Shen C, Liu J, Liu H, Li G, Wang H, Tian H, Mao Y, Hua D. Timosaponin AIII induces lipid peroxidation and ferroptosis by enhancing Rab7-mediated lipophagy in colorectal cancer cells. Phytomedicine. 2024;122: 155079. https://doi.org/10.1016/j.phymed.2023.155079.
10. Schuh R, Aicher W, Gaul U, Côté S, Preiss A, Maier D, Seifert E, Nauber U, Schröder C, Kemler R, et al. A conserved family of nuclear proteins containing structural elements of the finger protein encoded by Krüppel, a Drosophila segmentation gene. Cell. 1986;47(6):1025–32. https://doi.org/10.1016/0092-8674(86)90817-2.
11. Kremer-Tal S, Reeves HL, Narla G, Thung SN, Schwartz M, Difeo A, Katz A, Bruix J, Bioulac-Sage P, Martignetti JA, Friedman SL. Frequent inactivation of the tumor suppressor Kruppel-like factor 6 (KLF6) in hepatocellular carcinoma. Hepatology. 2004;40(5):1047–52. https://doi.org/10.1002/hep.20460.
12. Huang Z, He H, Qiu F, Qian H. Expression and prognosis value of the KLF family members in colorectal cancer. J Oncol. 2022;2022:6571272. https://doi.org/10.1155/2022/6571272.
13. Chen C, Hyytinen ER, Sun X, Helin HJ, Koivisto PA, Frierson HF Jr, Vessella RL, Dong JT. Deletion, mutation, and loss of expression of KLF6 in human prostate cancer. Am J Pathol. 2003;162(4):1349–54. https://doi.org/10.1016/S0002-9440(10)63930-2.
14. Ito G, Uchiyama M, Kondo M, Mori S, Usami N, Maeda O, Kawabe T, Hasegawa Y, Shimokata K, Sekido Y. Krüppel-like factor 6 is frequently down-regulated and induces apoptosis in non-small cell lung cancer cells. Cancer Res. 2004;64(11):3838–43. https://doi.org/10.1158/0008-5472.CAN-04-0185.
15. Sangodkar J, Shi J, DiFeo A, Schwartz R, Bromberg R, Choudhri A, McClinch K, Hatami R, Scheer E, Kremer-Tal S, Martignetti JA, Hui A, Leung WK, Friedman SL, Narla G. Functional role of the KLF6 tumour suppressor gene in gastric cancer. Eur J Cancer. 2009;45(4):666–76. https://doi.org/10.1016/j.ejca.2008.11.009.
16. Shi S, Li D, Li Y, Feng Z, Du Y, Nie Y. LncRNA CR749391 acts as a tumor suppressor to upregulate KLF6 expression via interacting with miR-181a in gastric cancer. Exp Ther Med. 2020;19(1):569–78. https://doi.org/10.3892/etm.2019.8226.
17. Wang Y, Lu K, Li W, Wang Z, Ding J, Zhu Z, Li Z. MiR-200c-3p aggravates gastric cell carcinoma via KLF6. Genes Genomics. 2021;43(11):1307–16. https://doi.org/10.1007/s13258-021-01160-6.
18. Lv J, Xie M, Zhao S, Qiu W, Wang S, Cao M. Nestin is essential for cellular redox homeostasis and gastric cancer metastasis through the mediation of the Keap1-Nrf2 axis. Cancer Cell Int. 2021;21(1):603. https://doi.org/10.1186/s12935-021-02184-4.
19. Fu D, Wang C, Yu L, Yu R. Induction of ferroptosis by ATF3 elevation alleviates cisplatin resistance in gastric cancer by restraining Nrf2/Keap1/xCT signaling. Cell Mol Biol Lett. 2021;26(1):26. https://doi.org/10.1186/s11658-021-00271-y.
20. Tong KI, Katoh Y, Kusunoki H, Itoh K, Tanaka T, Yamamoto M. Keap1 recruits Neh2 through binding to ETGE and DLG motifs: characterization of the two-site molecular recognition model. Mol Cell Biol. 2006;26(8):2887–900. https://doi.org/10.1128/MCB.26.8.2887-2900.2006.
21. Liu S, Pi J, Zhang Q. Signal amplification in the Keap1-Nrf2-ARE antioxidant response pathway. Redox Biol. 2022;54: 102389. https://doi.org/10.1016/j.redox.2022.102389.
22. Zhan T, Chen M, Liu W, Han Z, Zhu Q, Liu M, Tan J, Liu J, Chen X, Tian X, Huang X. MiR-455-3p inhibits gastric cancer progression by repressing Wnt/beta-catenin signaling through binding to ARMC8. BMC Med Genomics. 2023;16(1):155. https://doi.org/10.1186/s12920-023-01583-y.
23. Liu X, Pu K, Wang Y, Chen Y, Zhou Y. Gastric cancer-associated microRNA expression signatures: integrated bioinformatics analysis, validation, and clinical significance. Ann Transl Med. 2021;9(9):797. https://doi.org/10.21037/atm-21-1631.